Redox Biology 13 (2017) 288–300

Contents lists available at ScienceDirect

Redox Biology

journal homepage: www.elsevier.com/locate/redox

Research Paper

Nox2 contributes to hyperinsulinemia-induced redox imbalance and impaired vascular function

Abeer M. Mahmoud[a,b,c,*], Mohamed M. Ali[b,c], Edwin R. Miranda[a,c], Jacob T. Mey[a,c], Brian K. Blackburn[a,c], Jacob M. Haus[a,c], Shane A. Phillips[b,c,d,**]

[a] Department of Kinesiology and Nutrition, University of Illinois at Chicago, Chicago, IL, USA
[b] Department of Physical Therapy, University of Illinois at Chicago, Chicago, IL, USA
[c] Integrative Physiology Laboratory, College of Applied Health Sciences, University of Illinois at Chicago, Chicago, IL, USA
[d] Division of Endocrinology, Diabetes, and Metabolism, Department of Medicine, University of Illinois at Chicago, Chicago, IL, USA

ARTICLE INFO

Keywords:
Insulin
NADPH oxidase
Nitric oxide
Superoxide
Microvascular
Endothelial cells

ABSTRACT

Insulin resistance promotes vascular endothelial dysfunction and subsequent development of cardiovascular disease. Previously we found that skeletal muscle arteriolar flow-induced dilation (FID) was reduced following a hyperinsulinemic clamp in healthy adults. Therefore, we hypothesized that hyperinsulinemia, a hallmark of insulin resistance, contributes to microvascular endothelial cell dysfunction via inducing oxidative stress that is mediated by NADPH oxidase (Nox) system. We examined the effect of insulin, at levels that are comparable with human hyperinsulinemia on 1) FID of isolated arterioles from human skeletal muscle tissue in the presence and absence of Nox inhibitors and 2) human adipose microvascular endothelial cell (HAMECs) expression of nitric oxide (NO), endothelial NO synthase (eNOS), and Nox-mediated oxidative stress. In six lean healthy participants (mean age 25.5 ± 1.6 y, BMI 21.8 ± 0.9), reactive oxygen species (ROS) were increased while NO and arteriolar FID were reduced following 60 min of *ex vivo* insulin incubation. These changes were reversed after co-incubation with the Nox isoform 2 (Nox2) inhibitor, VAS2870. In HAMECs, insulin-induced time-dependent increases in Nox2 expression and $P47^{phox}$ phosphorylation were echoed by elevations of superoxide production. In contrast, phosphorylation of eNOS and expression of superoxide dismutase (SOD2 and SOD3) isoforms showed a biphasic response with an increased expression at earlier time points followed by a steep reduction phase. Insulin induced eNOS uncoupling that was synchronized with a drop of NO and a surge of ROS production. These effects were reversed by Tempol (SOD mimetic), Tetrahydrobiopterin (BH4; eNOS cofactor), and VAS2870. Finally, insulin induced nitrotyrosine formation which was reversed by inhibiting NO or superoxide generation. In conclusions, hyperinsulinemia may reduce FID via inducing Nox2-mediated superoxide production in microvascular endothelial cells which reduce the availability of NO and enhances peroxynitrite formation. Therefore, the Nox2 pathway should be considered as a target for the prevention of oxidative stress-associated endothelial dysfunction during hyperinsulinemia.

1. Introduction

An association between insulin resistance and the risk of developing cardiovascular disease (CVD) has been supported by epidemiological studies [1]. This association is based on the role of insulin in regulating the expression and function of a myriad of vasoactive substances and atherogenic-related factors [2,3]. The reduced response to insulin during insulin resistance promotes the beta cells of the pancreas to secrete increasing amounts of insulin, a condition that is known as hyperinsulinemia. However, the mechanistic role of hyperinsulinemia in promoting CVD is not clear due to the coexistence of other cardiovascular risk factors in insulin resistant patients such as obesity, type 2 diabetes, hypertension, and dyslipidemia [4].

Insulin has been shown to induce vasodilation via endothelial NO production however, it also prompts a simultaneous production of endothelin-1 (ET-1), a potent vasoconstrictive agent [3,5]. We previously

Abbreviations: CVD, cardiovascular disease; eNOS, endothelial nitric oxide synthase; ET-1, endothelin-1; FID, flow-induced dilation; H_2O_2, hydrogen peroxide; HAMECS, human adipose microvascular endothelial cells; NF-κB, Nuclear factor- κB; NO, nitric oxide; Nox, NADPH oxidase; ROS, reactive oxygen species; Ser, Serine; SOD, superoxide dismutase

* Correspondence to: Department of Kinesiology and Nutrition and Department of Physical Therapy, University of Illinois at Chicago, 1919 W. Taylor St. (AHSB), Room 506J, Chicago, IL 60612, USA.
** Correspondence to: Department of Physical Therapy, University of Illinois at Chicago, 1919 W. Taylor St. (AHSB), Room 746 (M/C 898), Chicago, IL 60612, USA.
E-mail addresses: amahmo4@uic.edu (A.M. Mahmoud), shanep@uic.edu (S.A. Phillips).

http://dx.doi.org/10.1016/j.redox.2017.06.001
Received 23 March 2017; Received in revised form 17 May 2017; Accepted 1 June 2017
Available online 03 June 2017
2213-2317/ © 2017 The Authors. Published by Elsevier B.V. This is an open access article under the CC BY-NC-ND license (http://creativecommons.org/licenses/BY-NC-ND/4.0/).

demonstrated that hyperinsulinemia disturbed the balance between these vasoactive mediators by augmenting the protein expression of ET-1 and ET receptor type A (ETAR) in human skeletal muscle tissue [6]. We also showed that hyperinsulinemia interfered with arteriolar vasodilation and NO bioavailability in obese, insulin resistant and lean healthy subjects [7]. Oxidative stress has been shown to contribute to the development of insulin resistance and ROS have been identified as critical signaling molecules in the development of metabolic and cardiovascular diseases [8]. Furthermore, oxidative stress might contribute to the disturbed production of NO and impaired vasodilation we demonstrated previously in the hyperinsulinemic states [6]. Accordingly, hyperinsulinemia may lead to an uninterrupted vicious cycle of oxidative stress and impaired insulin signaling which amplify the risk of developing CVD. In the current study, we extend our mechanistic inquiry of hyperinsulinemia-mediated vascular dysfunction via examination of ROS production and scavenging of NO.

Increased superoxide production has been linked to the impaired vascular dilatation through scavenging NO or interfering with NO synthesis and release [9]. NADPH oxidase is an enzyme complex that is responsible for superoxide production. This is followed by secondary generation of other ROS such as hydrogen peroxide (H_2O_2), hydroxyl radical, and hypochlorous acid, as well as peroxynitrite when NO is available [10]. Insulin can stimulate NADPH oxidase activity in human adipocytes [11] however, this mechanism has not been clearly demonstrated in microvascular tissue. The importance of testing insulin-induced redox signaling in microvascular tissue originates from the inherent sensitivity of this tissue to superoxide untoward effects that include impairing NO availability and microvascular function and thereby promoting increased peripheral vascular resistance [12]. Therefore, the purpose of the current study was to determine the effect of experimental hyperinsulinemia on Nox2 (the NADPH oxidase catalytic domain) signaling, superoxide generation and NO production in microvascular endothelial cells and isolated human skeletal muscle arterioles.

2. Materials and methods

2.1. Chemicals and reagents

Humulin R (insulin human recombinant) U-100 (100 U/ml) (Eli Lilly and Company, Indianapolis, IN) was used in the in vitro and FID experiments. NSC23766 trihydrochloride (Rac1 inhibitor), VAS2870 (Nox2 inhibitor), apocynin, (6 R)-5,6,7,8-Tetrahydrobiopterin dihydrochloride (BH4), 4-Hydroxy-TEMPO (Tempol), polyethylene glycol-catalase (PEG-catalase), and buthionine sulfoximine (BSO) were purchased from Sigma-Aldrich (St. Louis, MO). Nuclear factor- κB (NF-κB) SN50 cell permeable inhibitor peptide; AAVALLPAVLLALLAPVQRKRQKLMP was obtained from Santa Cruz Biotechnology (Dallas, TX). MitoSOX™ Red mitochondrial superoxide indicator and NO detection kit were obtained from Invitrogen Life Technologies (Carlsbad, CA) and Enzo Life Sciences (Farmingdale, NY), respectively.

2.2. Antibodies and DNA primers

Primers for Nox2 gene were designed using primer3 software and manufactured by Invitrogen Life Technologies (Forward: 5′ATGGTGGCATGGATGATTGC3′, Reverse: 5′TGACAACTCCAGTGATGCCT3′). NOS3 (H-159) rabbit polyclonal antibody was purchased from Santa Cruz Biotechnology. Phosphorylated eNOS (Serine (Ser)1177) rabbit monoclonal and nitrotyrosine rabbit polyclonal antibodies were purchased from Cell Signaling (Danvers, MA). Nox2 and Nox4 rabbit polyclonal antibodies were purchased from Abcam (Cambridge, MA). SOD2 rabbit monoclonal, SOD3 mouse monoclonal, and phosphorylated $p47^{phox}$ (Ser304) rabbit polyclonal antibodies were purchased from ThermoFisher Scientific (Waltham, MA).

2.3. Culture of human adipose microvascular endothelial cells (HAMECs)

HAMECs, primary endothelial cells, were obtained from the ATCC (Rockville, MD). Cells were maintained in phenol red-free endothelial cell medium (ECM) with L-glutamine supplemented with 5% fetal bovine serum, 1% endothelial cell growth supplement, and 1% penicillin/streptomycin solution (ScienCell Research Laboratories, Corte Del Cedro, CA). Passages 4–7 were used in the current experiments. Cells were incubated with insulin that covered a wide range of physiological and supraphysiological concentrations (1–100 nmol/L) used in the literature for endothelial cells [13–17]. Pre-incubations with Nox inhibitors (VAS2870 (2×10^{-6} mol/L) apocynin, (10^{-6} mol/L), and NSC23766 trihydrochloride (5×10^{-5} mol/L)) [18–22], PEG-catalase (500 U/ml), Tempol (10^{-5} mol/L), L-NAME (10^{-4} mol/L), or BH_4 (10^{-5} mol/L) were performed using the optimum concentrations that we reported in previous publications [23–26].

2.4. Nox2 silencing in HAMECs

HAMECs were seeded into 6-well plate at a concentration of 2×10^5 cells per well in 2 ml ECM growth medium and incubated at 37 C and 5% CO2. Twenty-four hours later, cells were transiently transfected with small interfering RNAs (siRNAs) pool that consists of three target-specific 19–25 nt siRNAs designed for effective knockdown of the Nox2 gene (Santa Cruz Biotechnology, Santa Cruz, CA). Transfection was performed following the standard protocol. Briefly, 1 μg of either the scrambled control siRNA or Nox2 siRNA was used in a total volume of 1 ml transfection media in which cells were incubated for 7 h. At the end of incubation period, transfection media were replaced with fresh growth media. 18 h later, cells were treated with insulin as described above. Validation of Nox2 knock-down was performed by western blot analysis of the total protein that was collected from transfected cells using a rabbit polyclonal Nox2 antibody (Abcam).

2.5. Immunoprecipitation

Immunoprecipitation (IP) of Nox2 was performed in total cell lysates using Dynabeads Protein G magnetic beads (Invitrogen Life Technologies). Dyna beads were incubated with the primary antibody for Nox2 or rabbit IgG (as a control for non-specific IgG binding) for one hour at room temperature then the complex was incubated with 200 μg of isolated cell protein overnight at 4 °C. The immunoprecipitate was eluted for downstream analysis of $p47^{phox}$ protein. Total cell lysate before IP (input) was used as a control for the efficiency and specificity of the IP process.

2.6. Western blot analysis

Total protein was isolated using RIPA lysis buffer (Cell Signaling) supplemented with protease and phosphatase inhibitor cocktail (MS-SAFE, Sigma-Aldrich). Protein concentration was measured using the Pierce BCA Protein Assay Kit (ThermoFisher Scientific). Proteins (10 μg) were resolved by 4–12% Bis-Tris gradient gels (Bio-Rad) and transferred to PVDF membranes. Membranes were blocked and incubated with primary antibodies overnight at 4 °C and then with infrared IRDye® - labeled secondary antibodies (LI-COR Biosciences, Lincoln, NE, USA) for 1 h at room temperature, protected from light. Membranes were washed with TBS + 0.1% Tween-20, dried for 1 h at room temperature and then scanned in the appropriate channel (700 nm for IRDye680TM antibodies, 800 nm for IRDye800TM antibodies) using an Odyssey Clx infrared imaging system. GAPDH rabbit polyclonal antibody (Cell Signaling) was used as a loading control. Images were then quantified using Image Studio ver. 4.0 (LI-COR) to calculate the intensity of the bands of the protein of interest relative to the expression of GAPDH from three independent experiments. Low-temperature SDS-PAGE (LT-PAGE) was performed for detection of

eNOS dimers using the previously reported procedures [27]. Briefly, total proteins were incubated in 1X Laemmli buffer without 2-mercaptoethanol at 37 °C for 5 min. The samples were then resolved on 4–12% Bis-Tris gradient gels (Bio-Rad). Gels and buffers were equilibrated at 4 °C before electrophoresis, and the buffer tank was placed in an ice bath during electrophoresis to maintain the temperature of the gel < 15 °C. Then, gels were transferred to PVDF membranes as a routine Western blot.

2.7. Real-time PCR

Total RNA was extracted using RNeasy mini kits (Qiagen, Germantown, MD). RNA quantity and quality was determined via spectrophotometer. Total RNA (5 μg) was reverse transcribed into cDNA using SuperScript RT III (Invitrogen). Target gene expression was determined via real-time RT-PCR using SYBR Green (Applied Biosystems, Foster City, CA) with custom designed primers. GAPDH was used as the housekeeping gene where the normalized expression ratio of the target genes was calculated using the $2^{-\Delta\Delta Ct}$ (Livak method) [28]. All reactions were carried out in triplicate from three independent experiments.

2.8. Nitric oxide and ROS detection

Nitric oxide and ROS generation were measured simultaneously in HAMECs using Enzo Life Sciences NO Detection Kit and ROS indicator (2′,7′-dichlorodihydrofluorescein diacetate (H2DCFDA); ThermoFisher Scientific). Briefly, cells were incubated with prediluted NO detection reagent (1:400) and 5 μmol/L ROS indicator for 1 h at 37 °C, protected from light. NO and ROS detection reagents were then removed and cells were washed and subsequently incubated with insulin (1 nmol/L) with and without BH4 (10^{-5} mol/L), VAS2870 (2×10^{-6} mol/L), NSC23766 trihydrochloride (5×10^{-5} mol/L), Tempol (10^{-5} mol/L), or PEG-catalase (500 U/ml) for 10–60 min. Untreated cells were used as a negative control and cells treated with L-arginine (10^{-5} mol/L) or BSO (10^{-3} mol/L) were used as positive controls for NO and ROS, respectively. At the end of each incubation period, cells were washed and imaged at 650/670 nm for NO detection and 495/527 nm for ROS detection (Eclipse TE 2000, Nikon, Japan). SpectraMax M Series Multi-Mode Microplate Reader (Molecular Devices, Fully Vale, CA) was used for quantification of the fluorescent signal.

2.9. Human participants

A cohort of 8 lean healthy participants (mean age 26 ± 2 y, BMI 21.8 ± 0.9 kg/m^2) were recruited from the Greater Chicago area for metabolic study and skeletal muscle biopsy. Subject exclusion criteria included the presence of acute or chronic illness, cardiac, pulmonary, liver, or kidney abnormalities, hypertension and tobacco use. Prior to testing procedures, subjects fasted overnight for a period of 10–12 h and were asked to refrain from physical activity outside of their normal activities. All participants logged their diet and physical activity habits for 3 days prior to testing and were also asked to refrain from consuming foods and beverages that contained caffeine (12 h prior) or alcohol (72 h prior). Body composition was measured using dual-energy x-ray absorptiometry (DEXA). All human procedures were approved by the University of Illinois at Chicago Institutional Review Board and written informed consent was obtained prior to participation.

2.10. Skeletal muscle biopsy

Skeletal muscle needle biopsies (vastus lateralis) were performed under local anesthetic (1% lidocaine) in the supine position after a period of 30 min rest to control for fluid volume shifts. Muscle tissue was immediately blotted, trimmed of adipose and connective tissue and immediately placed into cold HEPES buffer solution with a pH of 7.4 for FID experiments [6].

2.11. Microvascular preparation for FID measurements

Resistance arterioles, 40–50 μm diameter, and ≥ 2 mm length were carefully dissected from skeletal muscle tissue. Dissected arterioles were cleaned of fat and connective tissue and prepared for continuous measurement of lumen diameter as previously described [6,24]. In an organ perfusion chamber, vessels were cannulated with glass micropipettes (outer tip diameter ≤ 40 μm) filled with cold bicarbonate buffer (physiological salt solution) consisting of (mM) 123 NaCl, 4.4 KCL, 2.5 $CaCl_2$, 1.2 $MgSO_4$, 20 $NaHCO_3$, 1.2 KH_2PO_4, and 11 glucose. Both ends of the vessel were secured with 10-0 nylon Ethilon monofilament suture, and the vessels were maintained at an intraluminal pressure of 20 mmHg for 30 min. Each preparation was transferred to the stage of an inverted microscope (magnification × 200) attached to a video camera, video monitor, VCR recorder, and a video measuring device (model VIA-100; Boeckeler, Madison, WI). The external bathing medium was continuously superfused with heated buffer solution (pH = 7.4 ± 0.05, Po_2 = 140 ± 10 mmHg) aerated with a gas mixture of 21% O_2 5% CO_2 − 74% N_2 and maintained at 37 °C. Pressure was slowly increased to 100 mmHg and maintained for 30 min. Vessels were constricted 30–50% with endothelin-1 (Peninsula, San Carlos, CA). Vessels that did not constrict > 30% were excluded from the analysis. The flow was produced by simultaneously changing the heights of reservoirs in equal and opposite directions to generate a pressure gradient [29].

2.12. FID experimental protocols

Vessels were preconstricted with ET-1 incubation for 5 min, then the steady-state internal arterial diameter was measured before and during intraluminal flow corresponding to pressure gradients of 10–100 cmH_2O or increasing concentrations of acetylcholine (ACh; $10^{-9} - 10^{-4}$ M) [24]. This procedure was repeated after incubation with insulin (10 nmol/L) with and without the Nox2 inhibitor (VAS2870, 2×10^{-6} mol/L), Tempol (10^{-5} mol/L), the NOS inhibitor (L-NAME; 10^{-4} M), or the H_2O_2 scavenger pegylated (PEG)-catalase (500 U/ml) for 60 min. Maximal diameter of vessels was determined in the presence of papaverine (10^{-4} M). The % of vasodilation was calculated as the % of the ratio between the vessel's diameters in each treatment condition to the maximal diameter.

2.13. NO and ROS measurements in isolated microvessels

Nitric oxide and ROS generation were measured simultaneously in isolated skeletal muscle arterioles as previously described [30] using Enzo Life Sciences NO Detection Kit and ROS indicator (2′,7′-dichlorodihydrofluorescein diacetate (H_2DCFDA); ThermoFisher Scientific). Flow-induced nitric oxide and ROS production were measured in microvessels following cannulation and maintenance of 37 °C in a 20 ml aerated organ chambers, bathed in Krebs solution chamber at an equilibration pressure of 60 cm H_2O for 60 min. Vessels were incubated with insulin (1 nmol/L) with and without VAS2870, or Tempol. ACh (10^{-5} mol/L) and BSO (10^{-3} mol/L) were used as positive controls for NO and superoxide production, respectively. After 60 min, vessels were exposed to flow via a pressure gradient of Δ60 cm H_2O and subsequently excised, washed and mounted on slides. Mounted vessels were then imaged via fluorescence microscopy (Eclipse TE 2000, Nikon, Japan) at 650/670 nm for NO detection and 495/527 nm for ROS detection. Acquired images were analyzed for fluorescence intensity in arbitrary units using NIH Image J software (NIH, Bethesda, Maryland, USA).

2.14. Statistical analyses

Student's *t*-test was used for comparing different treatment

conditions and time points with the control in cell experiments. FID data collected at basal, insulin, insulin + VAS2870, and insulin + Tempol were compared using a one-way ANOVA with repeated measures for dose [Δ10, Δ20, Δ40, Δ60, Δ100 cmH2O]. Bonferroni/Dunn post-hoc tests were used for multiple comparisons when appropriate. All data represent mean ± standard error, and statistical significance was achieved if $p < 0.05$.

3. Results

3.1. Incubation with insulin impairs vasodilation of human skeletal muscle arterioles

Vasodilation of isolated arterioles incubated with insulin (10 nmol/L) for 10, 30, and 60 min was measured relative to basal conditions. The percentage of maximum dilation (MD) at Δ60 pressure gradient followed a biphasic pattern where FID was increased by 11% ($p = 0.01$) at 10 min and subsequently returned to baseline ($p = 0.07$) at 30 min (Fig. 1A). After 60 min of insulin incubation, % MD was reduced by 12% ($p = 0.004$) however, vasodilation was restored to basal levels when vessels were preincubated for 30-min with the Nox2 inhibitor, VAS2870 (2×10^{-6} mol/L) (% MD was increased by 20% relative to insulin alone, $p < 0.001$) (Fig. 1B). Similarly, inhibiting nuclear factor kappa B (NF-κB) via preincubation with SN50 cell permeable inhibitor peptide (15 μg/ml) resulted in improvement of arteriolar FID in response to insulin (17%, $p < 0.001$) (Fig. 1B). Incubation with catalase, an H_2O_2 scavenger, had no significant effect on the FID response relative to basal conditions however when combined with insulin, catalase resulted in more FID reductions compared to insulin alone ($p < 0.001$ at Δ100 pressure gradient) (Fig. 1C). FID was reduced at all pressure gradients after incubation with the NO synthesis inhibitor, L-NAME, for 60 min. The L-NAME-induced impairment in FID was 13% higher than that caused by insulin ($p < 0.001$) (Fig. 1D). In addition to measuring the FID, NO and ROS production in response to insulin was measured in the isolated skeletal muscle arterioles using fluorescent NO and ROS indicators. The signal intensity was measured using the NIH image J software. Fig. 2 shows that incubation with insulin increased ROS production at 30 min (103%, $p = 0.01$) and 60 min (1.9 folds, $p < 0.001$) (Figs. 2A and 2B). Pre-incubation with VAS2870 prevented any increases in ROS production at 60 min. As opposed to ROS, NO staining in isolated arterioles increased by 1.2 folds ($p = 0.001$) and 45% ($p = 0.02$) and decreased by 60% ($p < 0.001$) in response to insulin incubation for 10, 30, and 60 min, respectively (Figs. 2A and 2C). At 60 min, NO fluorescence improved by 2.7 folds when vessels were pre-incubated with VAS2870.

3.2. Insulin increased Nox2 expression and $p47^{phox}$ phosphorylation in HAMECs

To test dose-dependent effects of insulin, HAMECs were treated with a range of insulin concentrations (0.1–100 nmol/L). Total protein and mRNA were extracted from treated cells and analyzed for Nox2 expression. Lower levels of insulin did not change the Nox2 protein, however, 1 nmol/L which is representative of physiological

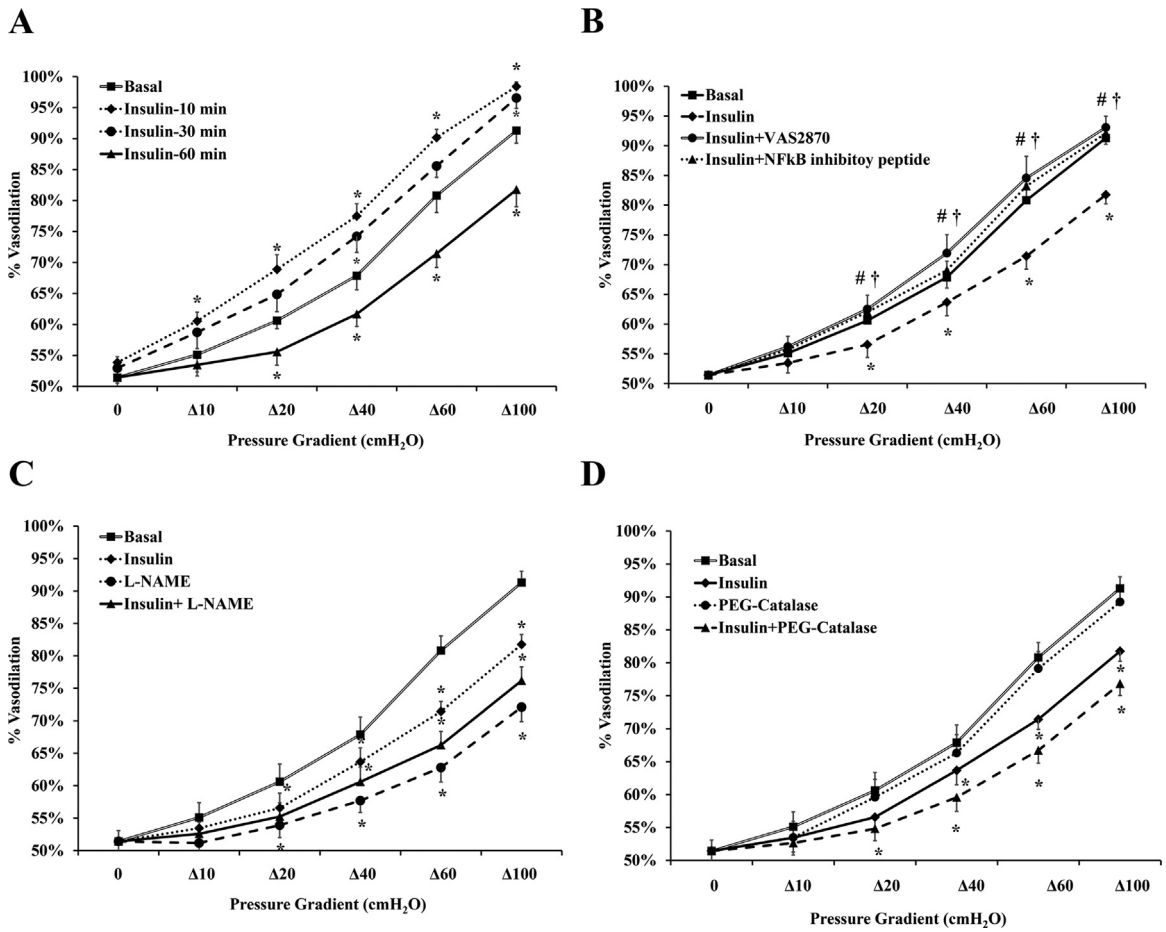

Fig. 1. Impaired FID in isolated skeletal muscle arterioles after incubation with insulin. FID was measured during intraluminal flow corresponding to pressure gradients of 10–100 cmH_2O in the absence or presence of insulin (10 nmol/L). (A) The effect of insulin on arteriolar FID at different time points (10, 30, and 60 min) ($n = 6$). (B) The effect of insulin on FID following a preincubation with the Nox2 inhibitor, VAS2870 or NF-κB inhibitory peptide ($n = 6$). (C) & (D) The effect of L-NAME and PEG-catalase on FID, respectively in the presence and absence of insulin ($n = 6$). All values are plotted as means ± SE. *($P < 0.05$) for comparison with baseline. † and # ($P < 0.05$) for insulin + VAS2870 and insulin + NF-κB vs insulin alone, respectively.

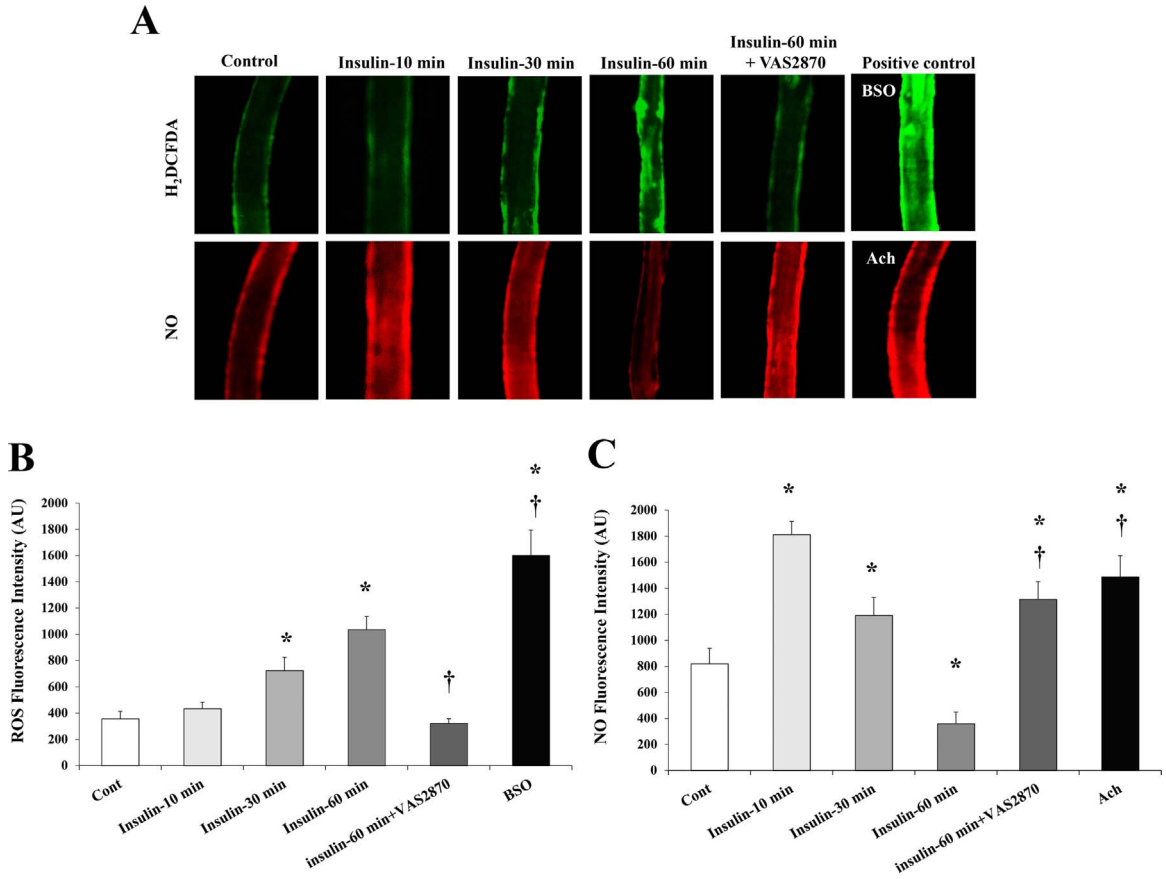

Fig. 2. ROS and NO production in isolated skeletal muscle arterioles in response to insulin. (A) Representative images of ROS and NO fluorescence in arterioles at baseline and after incubation with insulin (10 nmol/L) for 10–60 min or insulin (60 min) following a preincubation with VAS2870. BSO and Ach were used as positive controls for ROS and NO production, respectively. (B) & (C) Fluorescence intensities of ROS and NO were measured in arbitrary units using NIH Image J software. All values are plotted as means ± SE. *($P < 0.05$) for comparison with baseline. † ($P < 0.05$) for comparison with insulin. BSO, buthionine sulfoximine; Ach, acetylcholine.

hyperinsulinemia [3], increased Nox2 protein by 3 folds relative to basal levels ($p < 0.001$; Fig. 3A). Consistent with the protein responses, a corresponding 5-fold increase in Nox2 mRNA was observed at 1 nmol/L (Fig. 3C). We also tested the effect of insulin (1 nmol/L) on Nox2 protein levels at different time points that ranged from 30 min to 4 h. Insulin induced Nox2 protein levels by 28% at 30 min. This induction was time-dependent and reached up to 97% at 4 h (Fig. 3B). HAMECs were also analyzed for Nox isoform 4 (Nox4) protein expression in absence and presence of insulin (0.1–100 nmol/L) for different periods of incubation (30 min-4 h). Our data show that Nox4 protein is more abundant than Nox2 in HAMECs; the basal protein levels of Nox4 is 2-fold higher than Nox2. However, no significant changes were detected in Nox4 protein in response to insulin (Figs. 3A and 3B). It has been shown in previous studies that Nox2 activity is promoted by the binding of the regulatory subunit $p47^{phox}$ that is translocated from the cytoplasm to the cell membrane once phosphorylated [31]. Thus, we measured the phosphorylated fraction of $P47^{phox}$ (ser304) in response to insulin and tested its physical binding to Nox2 using the co-immunoprecipitation technique. Insulin's induction of $P47^{phox}$ phosphorylation started as early as 30 min (49%) and increased continuously with time (Fig. 3E). This induction was also dose-dependent and initiated at lower doses (0.1 nmol/L) than those observed to increase Nox2 protein levels, demonstrating a higher sensitivity of $P47^{phox}$ phosphorylation to insulin than Nox2 transcription (Fig. 3D). Also, corresponding doses of insulin increased levels of phosphorylated $P47^{phox}$ that were co-immunoprecipitated with Nox2 protein using Nox2 antibody (Fig. 3F), indicating an actual physical binding of the two domains which characterizes Nox2 activation.

3.3. Insulin induced time-dependent changes in ROS and protein levels of SOD2 and SOD3

We examined if insulin-mediated increases in Nox2 expression and activity augmented ROS generation in HAMECs. Levels of ROS were measured in response to increasing doses of insulin (0.01–100 nmol/L) using the cell-permeant ROS indicator, H_2DCFDA. Insulin was found to induce the production of ROS in a dose-dependent fashion starting from 1 nmol/L (107% at 30 min relative to baseline) (Fig. 4A and B). ROS production was reduced by 42% after inhibiting Nox2 using VAS2870, however, a minimal effect was achieved when H_2O_2 production was inhibited using catalase. This pattern was achieved across all time points but we only presented data for 30 min (Fig. 4C). Protein expression of SOD2 and SOD3 increased (2.2 folds and 56%, respectively) after 1 h of 1 nmol/L insulin incubation (Fig. 5A). However, after 4 h, SOD2 and SOD3 proteins were 27% and 40% lower than basal levels, respectively. Interrupting the superoxide production pathway by preincubation (30 min) with VAS2870 [18], apocynin, the Rac1 inhibitor, NSC23766, or Tempol prevented the suppressing effect of 4 h of insulin incubation on SOD2 and SOD3 proteins (Fig. 5B). For further verification of Nox2 involvement in insulin-mediated reductions of SOD2 and SOD3 protein levels, Nox2 expression was inhibited using a pool of three Nox2-targeting siRNAs. The efficiency of Nox2 silencing was confirmed by the significant reduction of Nox2 protein levels (91%, $p < 0.0001$) in Nox2 siRNA-transfected cells compared to non-transfected cells (control) and cells transected with scrambled sequences of siRNAs (scram-siRNA) (Fig. 5C). Nox2 silencing prevented insulin-induced reductions in SOD2 and SOD3 proteins and normalized their levels to the untreated control (Fig. 5D).

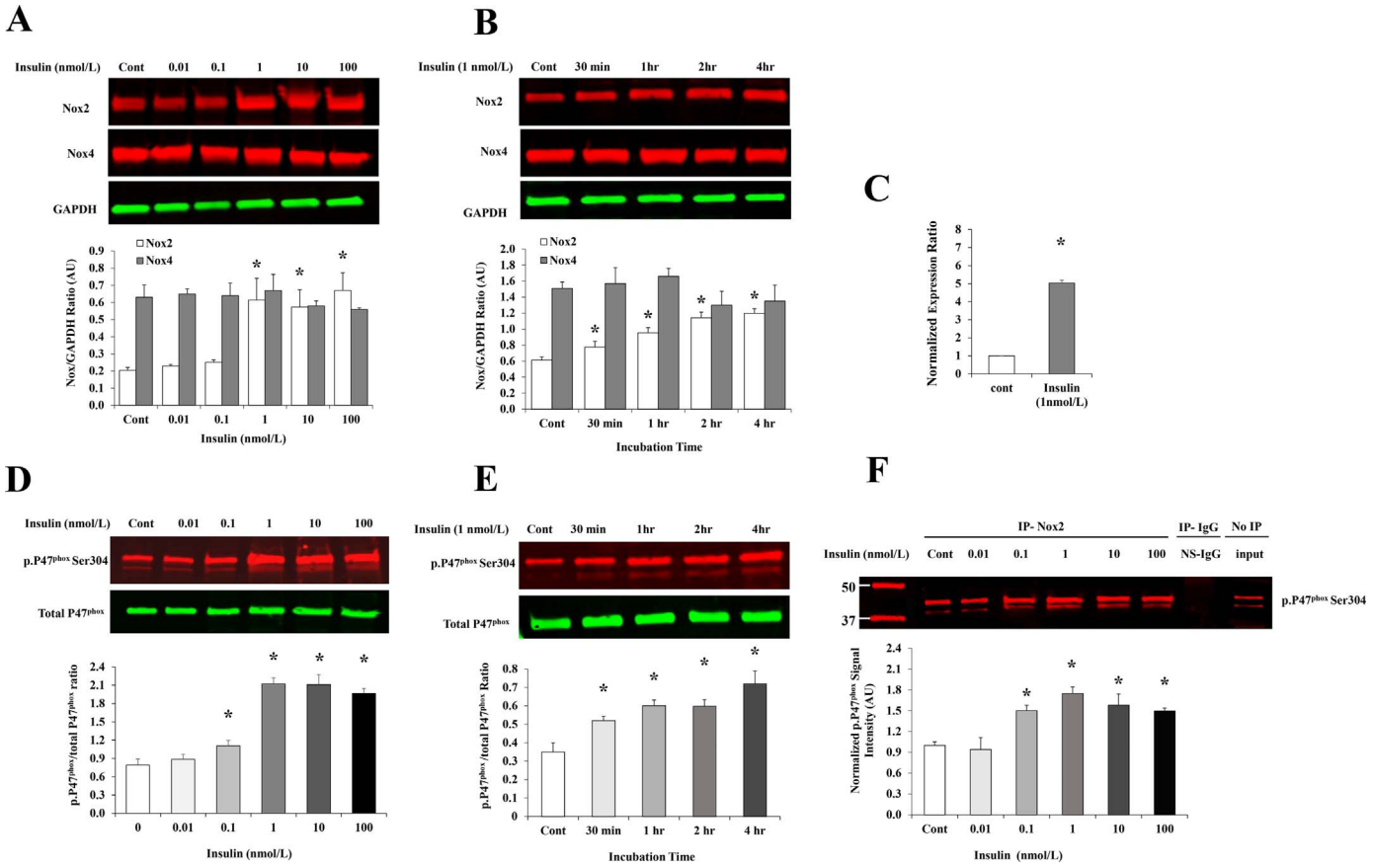

Fig. 3. Insulin induces Nox2 expression and P47^{phox} phosphorylation in HAMECs. (A) & (B) Western blot analysis and quantification of the normalized signal intensity of Nox2 and Nox4 protein in response to increasing doses of insulin (0.01–100 nmol/L) for 4 h and insulin (1 nmol/L) at different time points (30 min-4 h). (C) mRNA expression of Nox2 in response to insulin (1 nmol/L for 4 h). (D) & (E) Western blot analysis and quantification of the ratio between p. P47^{phox} and total P47^{phox} proteins in response to different doses of insulin (0.01–100 nmol/L for 4 h) and incubation periods (30 min-4 h) of 1 nmol/L insulin. (F) HAMECs treated with insulin (0.01–100 nmol/L for 4 h) were lysed, immunoprecipitated (IP) with Nox2 antibody or rabbit IgG (R-IgG) as a control for the non-specific IgG (NS-IgG) and immunoblotted for p. P47^{phox}. Untreated cells were used as a negative control and total cell lysate before IP was used to demonstrate that protein bands are corresponding to the expected molecular weight. Signal intensity of the IP Western bands were normalized to the untreated control (Cont). Images were then quantified using Image Studio ver. 4.0 (LI-COR). Results represent the means ± SE for three different experiments. *$p < 0.05$ for comparison with control.

3.4. Biphasic response of eNOS phosphorylation in response to insulin

The ability of insulin to induce eNOS phosphorylation via activating PI3K/Akt pathway has been verified in previous studies [2]. However, whether this response changes over a time course of insulin action has not been examined. Thus, we tested the effect of insulin (1 nmol/L) on eNOS phosphorylation at different time points (ranged from 30 min to 4 h). A biphasic pattern of eNOS (ser 1177) phosphorylation was observed in response to insulin treatment (1 nmol/L) with a maximum induction achieved at 1 h (7 folds) followed by 62% and 90% reductions of p.eNOS at 2 h and 4 h, respectively (Fig. 6A). Preincubation with Tempol, VAS2870, and BH4 increased the phosphorylated eNOS fraction after 4 h of insulin incubation by 2.3, 2.6, and 2.5 folds, respectively relative to insulin alone (Fig. 6B). Similarly, cells with silenced Nox2 expression had higher levels of eNOS phosphorylation in response to insulin incubation (1 nmol/L for 4 h) compared to non-transfected and scrambled siRNA-transfected cells (1.7 fold, $p = 0.005$) (Fig. 6C). Since uncoupling of eNOS has been linked to reduced eNOS activity and NO bioavailability [32], we measured levels of eNOS monomers and dimers in response to insulin treatment using low-temperature PAGE (LT-PAGE) as previously described [27] (Fig. 6D). Insulin (1nmol/L) induced time-dependent increases in eNOS monomer to dimer ratio starting as early as 30 min (22%) and increasing by 1.6 folds at 4 h. Co-incubation with Tempol (10 μmol/L), VAS2870 (2 μmol/L), or BH4 (10 μmol/L) reduced the eNOS monomer to dimer ratio by 69%, 63%, and 81%, respectively at 4 h compared with insulin treatment.

3.5. Insulin-induced NO production is interfered with by concomitant ROS generation

We next examined if the initial phase of insulin-mediated induction of eNOS phosphorylation was accompanied by an effective production of NO. Cells were probed with NO and ROS detection reagents after which, they were incubated with insulin (1 nmol/L) for 60 min. Visual and quantitative determination of NO and ROS production at basal, 10, 20, 30 and 60 min of insulin incubation were performed using a fluorescence microscope and a plate reader, respectively. Insulin induced NO production maximally at 20 min however at 30 min, NO production started to decrease and reached basal levels at 60 min (Fig. 7A). Generation of ROS in the same cell setting increased at 20 min and continued to increase at later time points (30 and 60 min). Our data clearly demonstrated that NO staining intensity dropped significantly as soon as ROS production surged. Then, the NO and ROS signals were quantified using a fluorescent plate reader and NO to ROS ratios were calculated (Fig. 7C). The NO/ROS ratio showed a biphasic pattern in response to insulin with a peak at 20 min followed by reductions at 30 and 60 min. Preincubation with the superoxide scavenger, Tempol (10 μmol/L), the Rac1 inhibitor, NSC23766 (50 μmol/L), or VAS2870 (2 μmol/L) improved the NO/ROS ratio at all time periods relative to insulin alone ($p < 0.05$). Similarly, inhibiting Nox2 expression via Nox2 siRNAs prevented the ROS surge and improved NO production at 60-min insulin incubation (Fig. 7B) and enhanced the NO/ROS ratio across all insulin incubation periods (10–60 min)

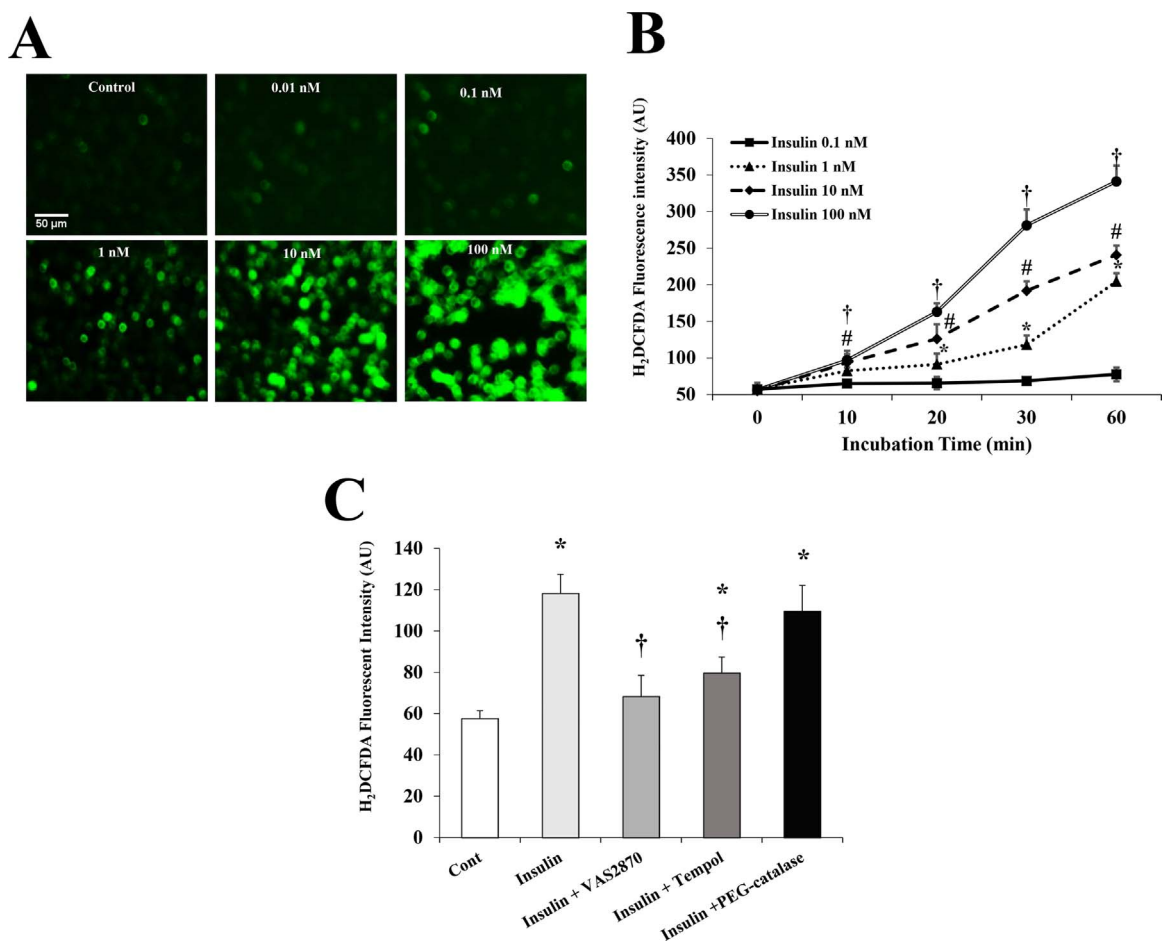

Fig. 4. Dose- and time-dependent effects of insulin on ROS production in HAMECs. (A) Visualization of ROS using H_2DCFDA fluorescent staining in HAMECs treated with insulin (0.01–100 nmol/L) for 30 min (B) Quantification of ROS fluorescent signal at different time points (0–60 min) using a multi-mode plate reader; *, #, † $p < 0.05$ for comparing signals at different time points with the baseline (0 min) at insulin doses 1, 10, and 100 nmol/L, respectively. (C) Quantification of ROS signal in HAMECs treated with insulin with and without antioxidants. All results represent the means ± SE for three different experiments. *$p < 0.05$ for comparison with control and † ($P < 0.05$) for comparison with insulin.

(Fig. 7D).

To this point, our data showed an increased production of both superoxide and NO as an initial response to high levels of insulin. Accordingly, we anticipated an enhanced formation of the cytotoxic oxidant peroxynitrite and we sought to measure nitrosylated proteins as a surrogate biomarker for peroxynitrite using an antibody that detects nitrotyrosine residues. Nitrotyrosine of insulin-stimulated (1nmol/l) HAMECs increased significantly after 2 h of insulin incubation (100%, $p < 0.001$) and persisted for 24 h (Fig. 8A). Insulin-induced formation of nitrotyrosine was reduced by 70–100% after inhibiting NO synthesis using L-NAME or interfering with superoxide formation by Nox2 inhibitors (VAS and apocynin), or Rac1 inhibitor (NSC23766) (Fig. 8B). These findings indicate that the concomitant induction of NO and superoxide by insulin promotes the formation of nitrosylated proteins, a process that is reserved by inhibiting either NO or superoxide.

4. Discussion

The major findings of this study are that insulin, at levels that are comparable to human hyperinsulinemia, impaired endothelial-mediated FID, reduced NO, and enhanced ROS production in isolated skeletal muscle arterioles. *In vitro* mechanistic studies using HAMECs demonstrated that insulin induced ROS formation mainly through increasing Nox2 expression and activity (as evidenced by increased $P47^{phox}$ phosphorylation) resulting in eNOS uncoupling, reduced NO generation, and altered metabolism of the available NO towards peroxynitrite formation. These data indicate that Nox2 may be a key player and a potential therapeutic target in hyperinsulinemia-associated microvascular dysfunction.

We previously showed that the baseline FID, measured *ex vivo* in isolated arterioles from skeletal muscle, is significantly lower in obese, insulin resistant subjects compared to lean healthy controls. These findings were consistent with prior studies that compared the in vivo-measured flow-mediated dilation between healthy and insulin resistant individuals (as reviewed by Reaven et al. [33]). We also showed that experimental hyperinsulinemia further impaired arteriolar FID in obese, insulin resistant subjects and reduced plasma NO levels [6]. The current study provides a possible mechanistic link between hyperinsulinemia and the impaired FID we reported previously and serves as a platform for future studies that target the induced Nox2 pathway in pathologic conditions characterized by hyperinsulinemia.

Recent evidence suggests a cross-talk between the ET-1 pathway and NADPH oxidase-derived superoxide production [34] and we previously demonstrated that hyperinsulinemia increases ET-1 levels in skeletal muscle tissues, inducing microvascular dysfunction [6]. Therefore, in the present study, we sought to further investigate the determinants of hyperinsulinemia-induced microvascular dysfunction by examining the contribution of NADPH oxidase-generated oxidative stress. H_2DCFDA fluorescence was used to assess oxidant generation in the vascular wall of isolated skeletal muscle arterioles. Arterioles that were incubated with insulin for 60 min demonstrated increased fluorescence compared with controls. Interestingly, incubation with Nox2 inhibitor, VAS2870 reduced the H_2DCFDA fluorescence suggesting that the main fraction of the generated ROS following hyperinsulinemia was

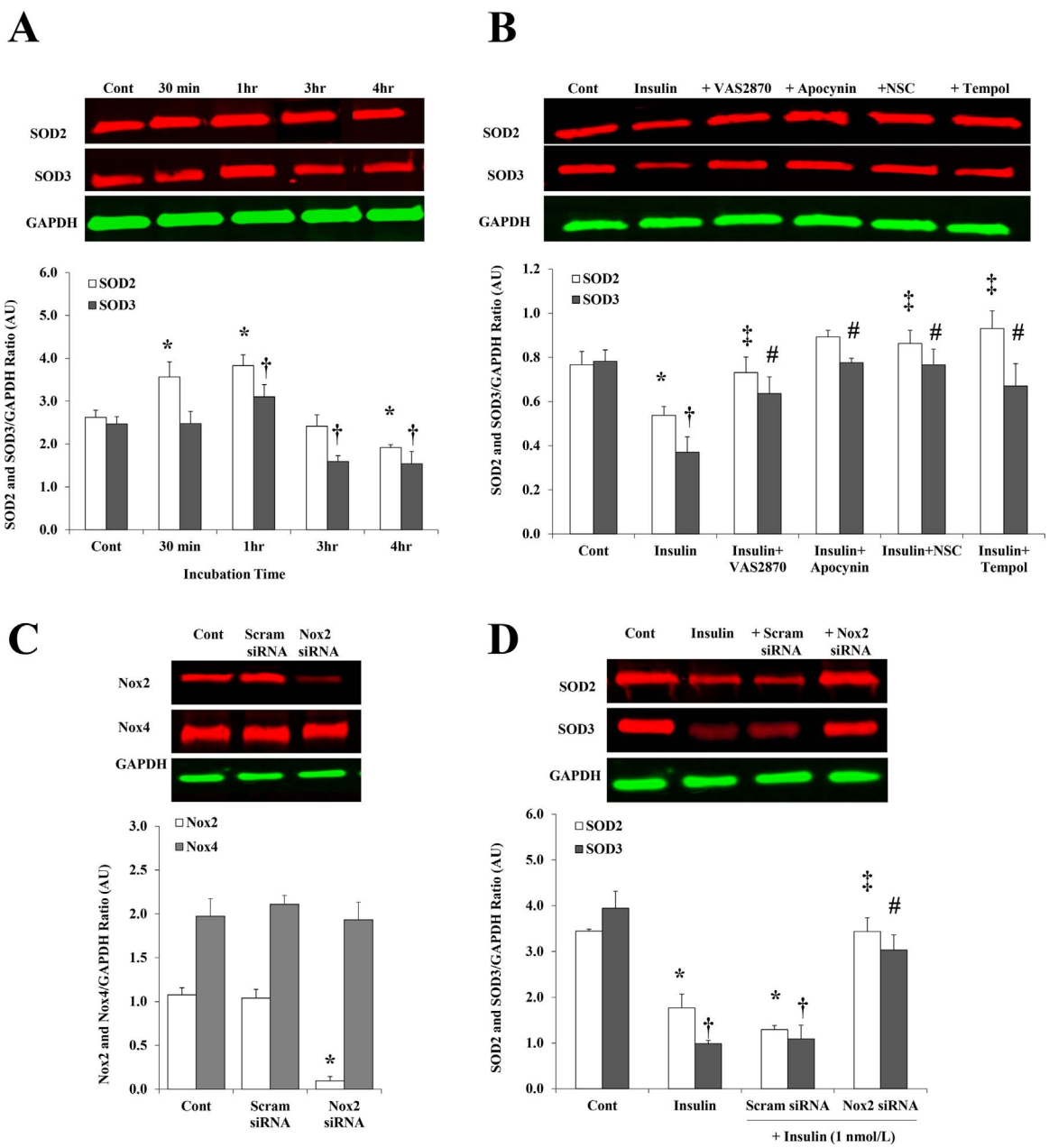

Fig. 5. Response of SOD2 and SOD3 proteins to insulin treatment in HAMECs. Western blot analysis and quantification of the relative signal intensity of SOD2 and SOD3 proteins in response to different incubation periods (30 min to 4 h) of 1 nmol/L insulin (A) and in response to insulin incubation (1 nmol/L) for 4 h along with the antioxidants, VAS2870, apocynin, NSC23766 trihydrochloride and Tempol (B). (C) Western blot analysis and quantification of the relative signal intensity of Nox2 and Nox4 proteins in cells transfected with Nox2 siRNA, cells transfected with a scrambled sequence of siRNA (scam) and non-transfected cells (cont). (D) Western blot analysis and quantification of the relative signal intensity of SOD2 and SOD3 proteins in response to insulin (1 nmol/L for 4hrs) in cells transfected with Nox2 siRNA, cells transfected with a scrambled sequence of siRNA (scam) and non-transfected cells (insulin). Untreated, non-transfected cells were used as a baseline control (cont). Results represent the means ± SE for three different experiments. * and † ($P < 0.05$) for comparison with control and ‡ and # ($P < 0.05$) for comparison with insulin for SOD2 and SOD3, respectively.

superoxide. Arteriolar FID was restored to the control level in vessels that were co-incubated with VAS2870 which confirms the role of superoxide in hyperinsulinemia-induced FID impairment. The lack of changes in FID after adding catalase supports our assumption that insulin-mediated FID changes are mainly attributable to superoxide production and not H_2O_2. In insulin-treated vessels, NO production was also improved with anti-oxidant co-incubation.

Nox2 is a prominent source of superoxide formation in endothelial cells and appears to be the major source of ROS generation during hypertension [35]. In concordance with these clinical findings, we found that endothelial stimulation with insulin induced dose- and time-dependent increases in the Nox2 expression and the phosphorylation of its regulatory subunit, $P47^{phox}$ which supports the contribution of this system to insulin-induced ROS formation. Nox2 was the first Nox isoform to be identified in endothelial cells and has been shown to be the most important in the context of vascular pathology [36]. Relatively recently, Nox4 was shown to be the most highly expressed Nox isoform in endothelial cells [37–39]. However, previous studies that have examined expression levels of Nox isoforms in the vascular wall in experimental models of hypertension, hypercholesterolemia, diabetes, obesity, and also in humans with coronary artery disease reported increases in the expression of Nox2 and its regulatory subunits and no changes in Nox4 expression [36,40–42]. Moreover, studies in transgenic mice indicate that Nox2 activity contribute to vascular pathology while Nox4 activity is necessary for vascular activity and function [43,44]. This was also supported by studies demonstrating that Nox2

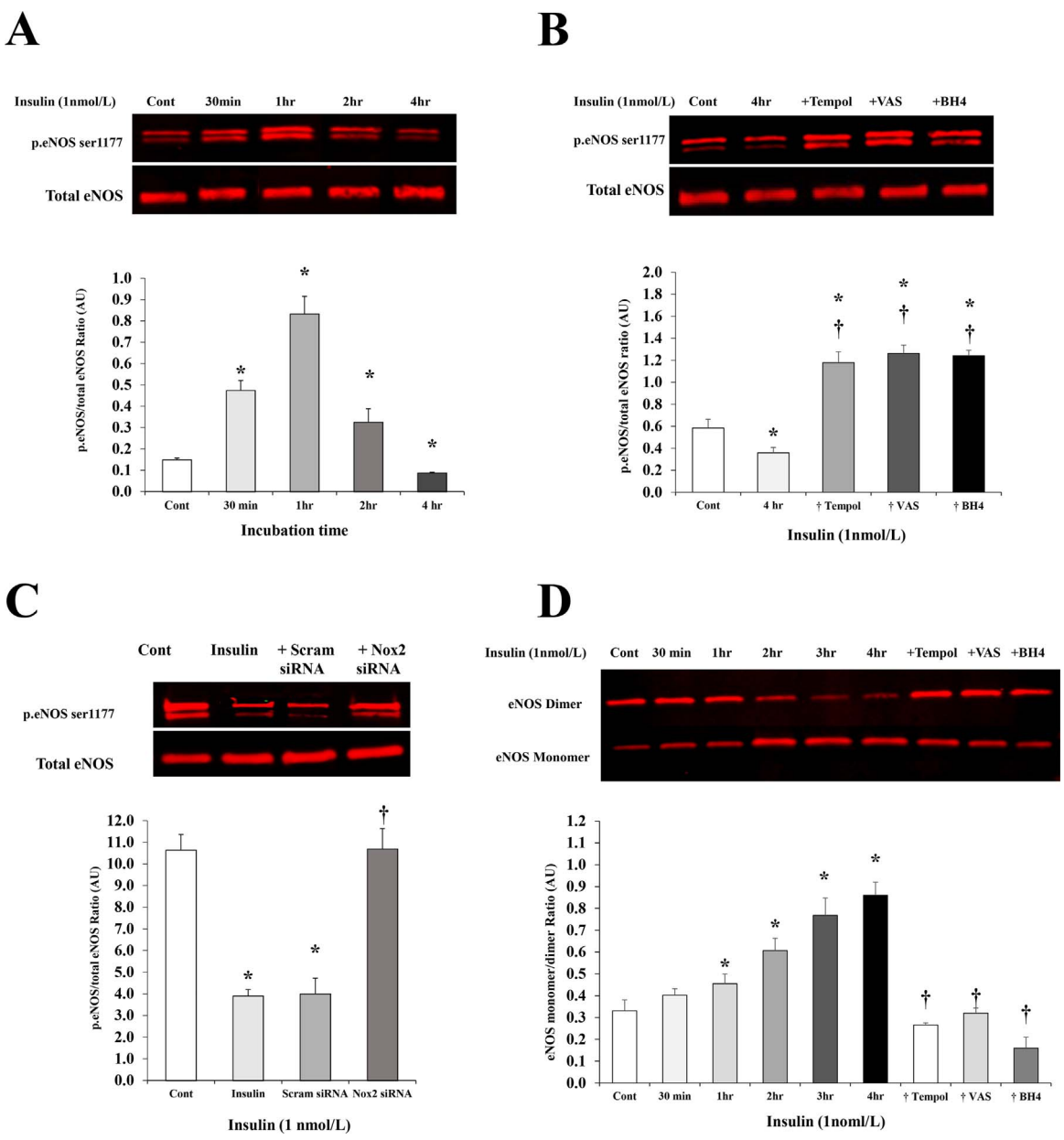

Fig. 6. The effect of insulin on eNOS phosphorylation and uncoupling. Western blot analysis and quantification of the relative signal intensity of phosphorylated eNOS (ser 1177) protein to total eNOS in response to incubation with insulin (1nmol/L) for different time periods (30 min to 4 h) (A) and in response to insulin incubation for 4 h along with the antioxidants, Tempol, VAS2870, and BH4 (B). (C) Western blot analysis and quantification of the relative signal intensity of phosphorylated eNOS in response to insulin (1 nmol/L for 4hrs) in cells transfected with Nox2 siRNA, cells transfected with a scrambled sequence of siRNA (scam) and non-transfected cells (insulin). Untreated, non-transfected cells were used as a baseline control (cont). (D) Western blot analysis using low-temperature SDS-PAGE (LT-PAGE) to assess eNOS monomer to dimer ratio in HAMECs treated with insulin (1 nmol/L) for 30 min to 4 h and with insulin plus Tempol, VAS2870, or BH4 for 4 h. Results represent the means ± SE for three different experiments. *($P < 0.05$) for comparison with control. † ($P < 0.05$) for comparison with insulin.

activation correlated with superoxide generation while Nox4 correlated with a spontaneous release of H_2O_2 [45]; the latter is a hyperpolarizing factor with a critical role in vascular homeostasis and vasodilation as was comprehensively reviewed in Breton-Romero et al. [46]. In support of this evidence, our data showed that Nox2 is the major contributor in insulin-induced oxidative stress in endothelial cells. Although basal levels of Nox4 protein in endothelial cells were two-fold higher than Nox2 as shown in Fig. 3, Nox4 protein did not increase in response to high levels of insulin. Furthermore, specific knock down of Nox2 gene and inhibition of Rac1, which is necessary only for Nox2 activation and not Nox4 [37], interfered with insulin-induced ROS production (Fig. 7) indicating that the major part of insulin-induced oxidative stress in endothelial cells is mediated via Nox2 isoform. Yet, a possible role for Nox4 or the other endothelial-expressed isoforms (e.g. Nox1 and Nox5) in vascular dysfunction cannot be completely disregarded and further investigations to elucidate this role are encouraged.

Oxidative stress is characterized by imbalanced ROS production and antioxidant defenses such as the SODs. Among these enzymes are manganese-dependent SOD (MnSOD or SOD2) which plays a major role due to its mitochondrial location where most of the superoxide is produced and copper/zinc-dependent extracellular SOD (Cu/ZnSOD or SOD3). In the present study, insulin increased SOD2 and SOD3 proteins after 1 h. We believe that this initial induction of SOD levels is a response to the increased superoxide production as evidenced by its abolishment by the antioxidants, VAS2870, NSC23766, and NF-κB inhibitory peptide. Unlike the continuous time-dependent increases in Nox2 activity and superoxide production in response to insulin, SOD2 and SOD3 proteins exhibited a biphasic pattern with a significant steep

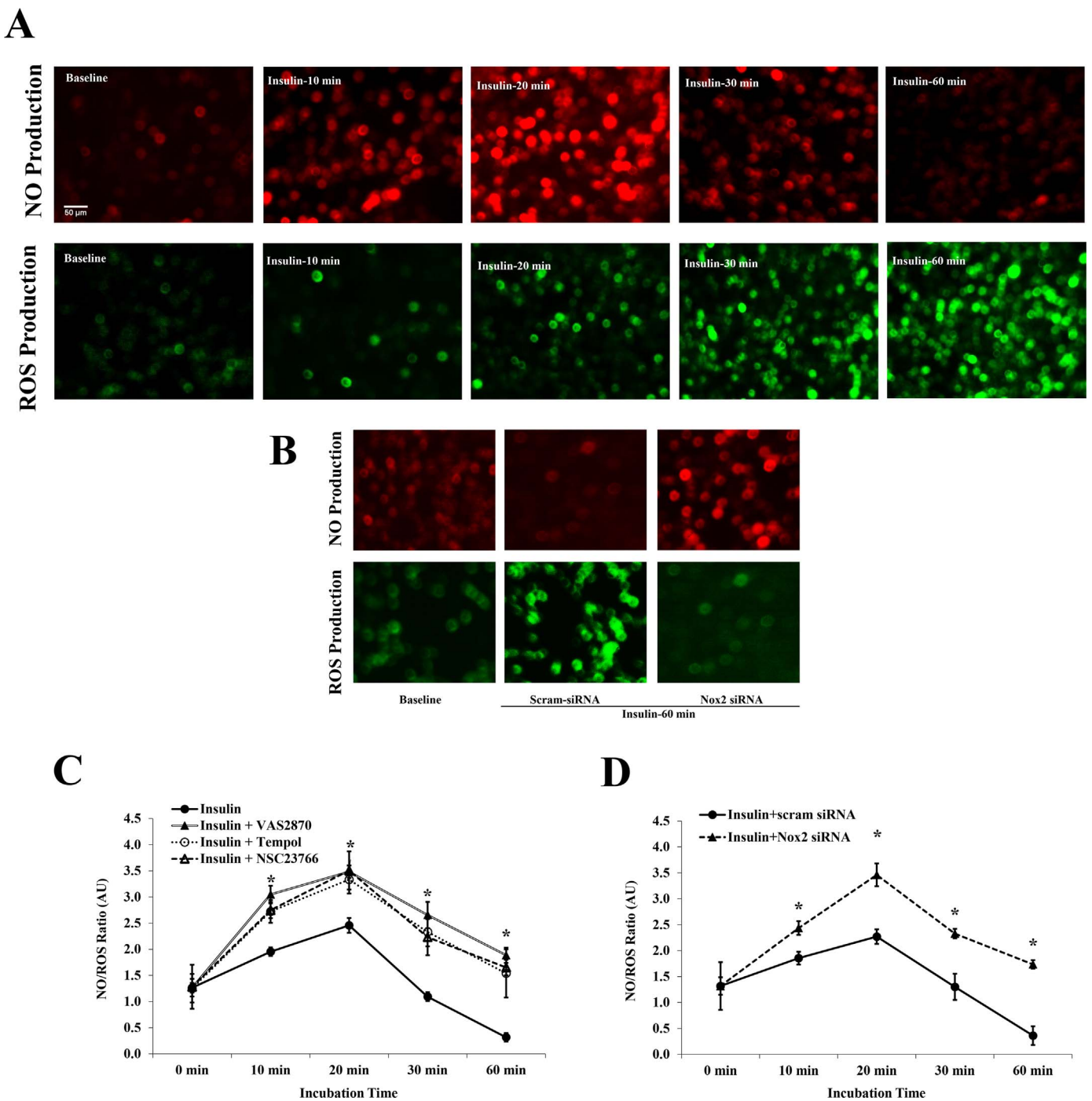

Fig. 7. Transient induction of NO levels in HAMECs in response to insulin. (A) Visualization of NO and ROS in HAMECs using NO detector and H_2DCFDA fluorescent staining, respectively at baseline (1st column) or in response to insulin (1nmol/L) for 20 min (2nd column), 30 min (3rd column), and 60 min (4th column). (B) Visualization of NO and ROS in HAMECs at baseline (1st column) or in response to insulin (1nmol/L) for 60 min in scram siRNA-transfected cells (2nd column) and Nox2 siRNA-transfected cells (3rd column). (C) Quantification of NO to ROS fluorescence intensity ratio in HAMECs in response to insulin (1 nmol/L) at incubation periods that ranged from 0 to 60 min with and without VAS2870, Tempol, and NSC23766 trihydrochloride. (D) Quantification of NO to ROS fluorescence intensity ratio in HAMECs in response to insulin (1 nmol/L) at incubation periods that ranged from 0 to 60 min in scram siRNA and Nox2 siRNA-transfected cells. (* $p < 0.05$) for comparison with insulin in (C) and for comparison with scram-siRNA in (D).

reduction after 2 h of insulin incubation. This imbalance may result in an unopposed production of superoxide and further impairments of vascular function at later time points. The reason behind the reduction of SOD expression in prolonged oxidative stress conditions is not well understood, however, previous studies have suggested that SOD undergoes irreversible inactivation by the accumulation of its product, H_2O_2 [47,48]. Accompanying the loss of activity, SOD also undergoes proteolysis and degradation, an effect that was inhibited by ROS scavengers such as ascorbate [49].

The effect of insulin on eNOS phosphorylation appears to be time-sensitive which might explain, at least in part, the discrepancy among some clinical and experimental studies that assessed vascular consequences of hyperinsulinemia using different time points [3]. The response of eNOS phosphorylation to insulin followed a biphasic pattern where it showed reductions at later time points. This reduction synchronized with the decrease in SOD2 and SOD3 proteins suggesting a possible protective effect of SODs on eNOS phosphorylation. The reduction in SODs along with the continued production of superoxide

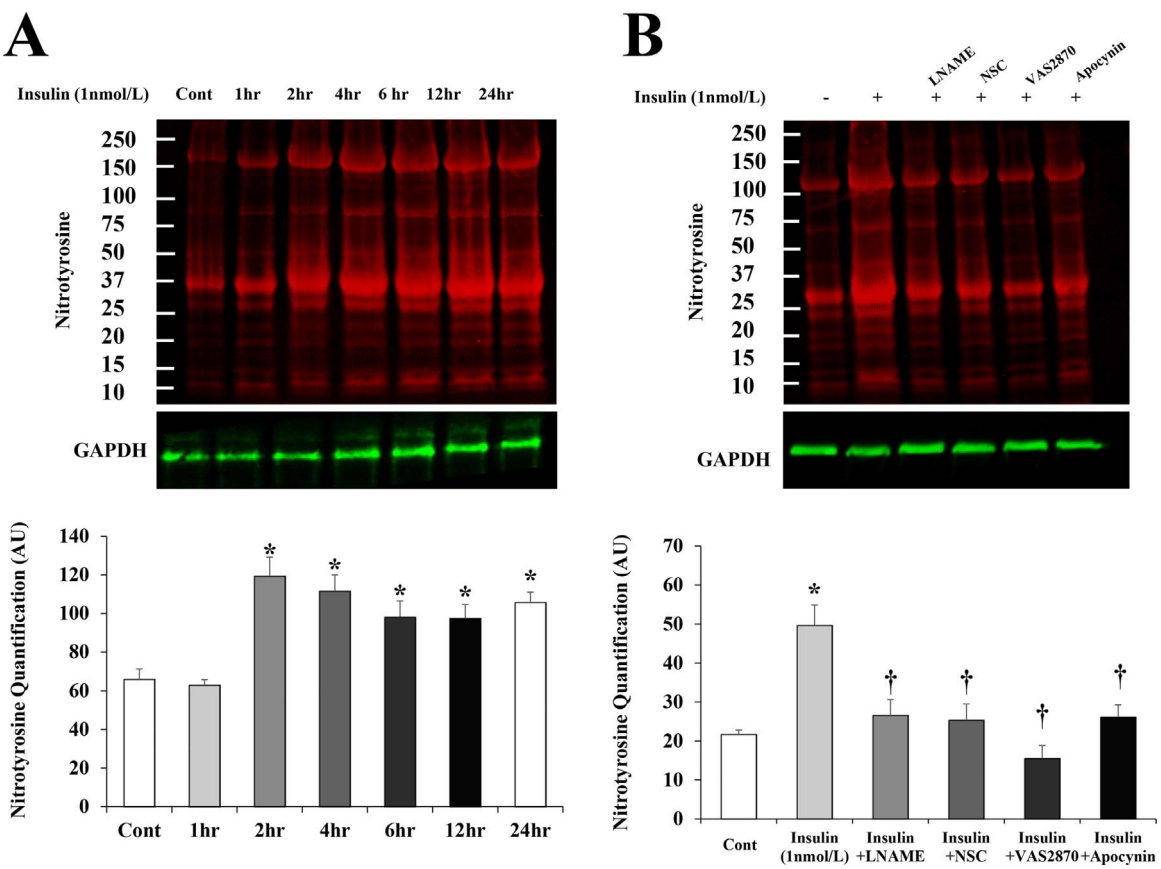

Fig. 8. Persistent increases in nitrosylated proteins after insulin incubation. Western blot analysis and quantification of the relative signal intensity of nitrotyrosine in HAMECs treated with insulin (1 nmol/L) for 1–24 h (A) or insulin plus L-NAME, VAS2870, NSC23766 trihydrochloride, or apocynin for 4 h (B). Results represent the means ± SE for three different experiments. *($P < 0.05$) for comparison with control. † ($P < 0.05$) for comparison with insulin.

results in eNOS uncoupling as showed in Fig. 6D which, in turn, inhibits eNOS phosphorylation and NO production. One way superoxide causes eNOS uncoupling is by oxidizing the eNOS cofactor, BH4 to BH2 resulting in inhibition of eNOS dimerization and subsequently preventing its phosphorylation [32]. In support of this notion, we demonstrated reductions in eNOS uncoupling and increases in eNOS phosphorylation when BH4 was exogenously supplied.

Per our data, the biphasic pattern of eNOS activity was accompanied by a biphasic NO response. However, the reduction in NO levels started at earlier time points (30 min) than reductions in eNOS phosphorylation or eNOS uncoupling (2 h). This lack of correlation between the intact eNOS activity, as indicated by eNOS phosphorylation and dimerization, and NO production after 1 h of insulin incubation could be related to the ROS surge at this time point. It is likely that the coexistence of ROS scavenges reduces NO availability even before eNOS activity is impaired. Previous studies reported extremely high affinity and rapid interaction between ROS and NO [50] indicating that the effect of ROS on lowering NO availability might precede its suppressive effect on eNOS activity. However, further studies are needed to dissect the direct effect of hyperinsulinemia-induced ROS on NO from that mediated by the suppression of eNOS activity.

When superoxide quenches NO it forms peroxynitrite which itself is a potent cytotoxic oxidant that modifies tyrosine residues into nitrotyrosine [51]. This nitration process damages several structural proteins and other proteins that are involved in metabolism, calcium homeostasis and oxidative responses resulting in major pathological consequences [52]. Previous studies reported a role of nitration in human atherosclerosis, myocardial ischemia, and other inflammatory and cardiovascular morbidities [53,54]. In our study, we showed that endothelial stimulation with insulin levels that are corresponding to hyperinsulinemia induced nitrotyrosine formation leaving a footprint that was detectable in endothelial cells for an extended time period. The formation of nitrotyrosine was prevented by either LNAME or antioxidants, supporting the assumption that the co-existence of NO and superoxide in the system is behind this detrimental protein modification. One may ask why SODs did not protect NO from being oxidized by superoxide radicals. While the answer to this question was beyond the focus of the present investigation, previous studies have described NO as a powerful competitor for superoxide binding; the binding between superoxide and NO is 7000 times faster than that between superoxide and SOD [50]. Coupled with evidence in the present study, indicating nitrotyrosine formation increased at time points concurrent with maximum SOD expression (1–3 h), it is possible that SOD system is inefficient when excess NO is in the vicinity competing for superoxide binding.

In summary, insulin at levels that are corresponding to the reported compensatory hyperinsulinemia in insulin-resistant individuals may induce Nox2-mediated oxidative stress that alters eNOS phosphorylation, NO availability, and ultimately impairs vasodilation. Also, at these levels, insulin induces long-lasting protein nitration that is known to compromise the function of critical structural and metabolic proteins. A limitation of this study could be the use of in vitro endothelial cell model. While endothelial cell models are powerful assessment tools that help to provide mechanistic insight into CVD development, we must acknowledge that these models, by design, set aside the tissue of interest from the rest of the body removing systemic influences. Accordingly, results from such in vitro studies should be interpreted cautiously. For instance, in the human body NO is removed within seconds by diffusion through tissues to enter red blood cells and react with oxyhemoglobin. This drain system is lacking in the in vitro model which allows NO to persist for several minutes. Regardless, knowing that the interaction between NO and superoxide occurs in the first few

milliseconds after NO is produced may indicate that the absence of a drain in the endothelial cells is less likely to change the outcome. Vasodilation is the physiological composite of interactions between endothelial and smooth muscle cells in the vascular wall. Thus, integrated models that contain multiple cell types or whole organ studies would be a better step towards improving our investigation tools. To that end, the strength of the current study is the use of an *ex vivo* model of isolated arterioles from human skeletal muscle to support our findings in the endothelial cells.

In conclusion, the present investigation suggests that the increased risk of microvascular endothelial dysfunction during insulin resistance be perpetuated by the accompanying hyperinsulinemia-induced NADPH oxidase activity. Indeed, this study directs the attention towards hyperinsulinemia as a major factor that can induce redox imbalance and microvascular dysfunction in absence of other metabolic disorders. This might include not only the compensatory hyperinsulinemia but also the iatrogenic hyperinsulinemia that may occur secondary to therapeutic approaches involving insulin secretagogues and administration of exogenous insulin.

Funding

This research was supported by the following funding sources: NIH R01s HL095701, HL130513A1 (SAP), American Diabetes Association Grant 1-14-JF-32 (JMH), and American Heart Association Grant 15POST24480172 (AMM).

Declaration of interest

No potential conflicts of interest were disclosed.

Acknowledgments

The authors would like to thank the research participants and the nursing staff of the Clinical Research Centers of the University of Illinois at Chicago.

References

[1] G. Garcia-Romero, H.F. Escobar-Morreale, Hyperandrogenism, insulin resistance and hyperinsulinemia as cardiovascular risk factors in diabetes mellitus, Curr. Diabetes Rev. 2 (1) (2006) 39–49.
[2] A.D. Baron, Hemodynamic actions of insulin, Am. J. Physiol. 267 (2 Pt 1) (1994) E187–E202.
[3] A.M. Mahmoud, M.D. Brown, S.A. Phillips, et al., Skeletal muscle vascular function: a counterbalance of insulin action, Microcirculation 22 (5) (2015) 327–347.
[4] S.H. Kim, G.M. Reaven, Insulin resistance and hyperinsulinemia: you can't have one without the other, Diabetes Care 31 (7) (2008) 1433–1438.
[5] R. Muniyappa, M. Montagnani, K.K. Koh, et al., Cardiovascular actions of insulin, Endocr. Rev. 28 (5) (2007) 463–491.
[6] A.M. Mahmoud, M.R. Szczurek, B.K. Blackburn, et al., Hyperinsulinemia augments endothelin-1 protein expression and impairs vasodilation of human skeletal muscle arterioles, Physiol. Rep. 4 (2016) 16.
[7] T.P. Solomon, J.M. Haus, Y. Li, et al., Progressive hyperglycemia across the glucose tolerance continuum in older obese adults is related to skeletal muscle capillarization and nitric oxide bioavailability, J. Clin. Endocrinol. Metab. 96 (5) (2011) 1377–1384.
[8] K. Park, M. Gross, D.H. Lee, et al., Oxidative stress and insulin resistance: the coronary artery risk development in young adults study, Diabetes Care 32 (7) (2009) 1302–1307.
[9] J.H. Pinkney, C.D. Stehouwer, S.W. Coppack, et al., Endothelial dysfunction: cause of the insulin resistance syndrome, Diabetes 46 (Suppl 2) (1997) S9–S13.
[10] J.D. Lambeth, NOX enzymes and the biology of reactive oxygen, Nat. Rev. Immunol. 4 (3) (2004) 181–189.
[11] H.I. Krieger-Brauer, P.K. Medda, H. Kather, Insulin-induced activation of NADPH-dependent H2O2 generation in human adipocyte plasma membranes is mediated by Galphai2, J. Biol. Chem. 272 (15) (1997) 10135–10143.
[12] R. Madonna, R. De Caterina, Cellular and molecular mechanisms of vascular injury in diabetes–part I: pathways of vascular disease in diabetes, Vasc. Pharmacol. 54 (3–6) (2011) 68–74.
[13] J.W. Langston, W. Li, L. Harrison, et al., Activation of promoter activity of the catalytic subunit of gamma-glutamylcysteine ligase (GCL) in brain endothelial cells by insulin requires antioxidant response element 4 and altered glycemic status: implication for GCL expression and GSH synthesis, Free Radic. Biol. Med. 51 (9) (2011) 1749–1757.
[14] Y. Liu, M. Petreaca, M. Martins-Green, Cell and molecular mechanisms of insulin-induced angiogenesis, J. Cell Mol. Med. 13 (11–12) (2009) 4492–4504.
[15] J. Li, C. Jin, J.C. Cleveland Jr.et al., Enhanced inflammatory responses to toll-like receptor 2/4 stimulation in type 1 diabetic coronary artery endothelial cells: the effect of insulin, Cardiovasc. Diabetol. 9 (2010) 90.
[16] S. Guo, M.J. Philbrick, X. An, et al., Response gene to complement 32 (RGC-32) in endothelial cells is induced by glucose and helpful to maintain glucose homeostasis, Int. J. Clin. Exp. Med. 7 (9) (2014) 2541–2549.
[17] A.J. Genders, V. Frison, S.R. Abramson, et al., Endothelial cells actively concentrate insulin during its transendothelial transport, Microcirculation 20 (5) (2013) 434–439.
[18] J.H. Leusen, K. Fluiter, P.M. Hilarius, et al., Interactions between the cytosolic components p47phox and p67phox of the human neutrophil NADPH oxidase that are not required for activation in the cell-free system, J. Biol. Chem. 270 (19) (1995) 11216–11221.
[19] H. ten Freyhaus, M. Huntgeburth, K. Wingler, et al., Novel Nox inhibitor VAS2870 attenuates PDGF-dependent smooth muscle cell chemotaxis, but not proliferation, Cardiovasc. Res. 71 (2) (2006) 331–341.
[20] M. El Assar, J. Angulo, M. Santos-Ruiz, et al., Differential effect of amylin on endothelial-dependent vasodilation in mesenteric arteries from control and insulin resistant rats, PLoS One 10 (3) (2015) e0120479.
[21] M.H. Tsai, M.J. Jiang, Reactive oxygen species are involved in regulating alpha1-adrenoceptor-activated vascular smooth muscle contraction, J. Biomed. Sci. 17 (2010) 67.
[22] T. Speer, L. Rohrer, P. Blyszczuk, et al., Abnormal high-density lipoprotein induces endothelial dysfunction via activation of Toll-like receptor-2, Immunity 38 (4) (2013) 754–768.
[23] R.Q. Migrino, S. Truran, D.D. Gutterman, et al., Human microvascular dysfunction and apoptotic injury induced by AL amyloidosis light chain proteins, Am. J. Physiol. Heart Circ. Physiol. 301 (6) (2011) H2305–H2312.
[24] S.A. Phillips, O.A. Hatoum, D.D. Gutterman, The mechanism of flow-induced dilation in human adipose arterioles involves hydrogen peroxide during CAD, Am. J. Physiol. Heart Circ. Physiol. 292 (1) (2007) H93–H100.
[25] A. Cavka, I. Jukic, M. Ali, et al., Short-term high salt intake reduces brachial artery and microvascular function in the absence of changes in blood pressure, J. Hypertens. 34 (4) (2016) 676–684.
[26] A.M. Beyer, M.J. Durand, J. Hockenberry, et al., An acute rise in intraluminal pressure shifts the mediator of flow-mediated dilation from nitric oxide to hydrogen peroxide in human arterioles, Am. J. Physiol. Heart Circ. Physiol. 307 (11) (2014) H1587–H1593.
[27] P. Klatt, K. Schmidt, D. Lehner, et al., Structural analysis of porcine brain nitric oxide synthase reveals a role for tetrahydrobiopterin and L-arginine in the formation of an SDS-resistant dimer, EMBO J. 14 (15) (1995) 3687–3695.
[28] K.J. Livak, T.D. Schmittgen, Analysis of relative gene expression data using real-time quantitative PCR and the 2(-Delta Delta C(T)) Method, Methods 25 (4) (2001) 402–408.
[29] H. Miura, R.E. Wachtel, Y. Liu, et al., Flow-induced dilation of human coronary arterioles: important role of Ca(2+)-activated K(+) channels, Circulation 103 (15) (2001) 1992–1998.
[30] A.T. Robinson, N.C. Franklin, E. Norkeviciute, et al., Improved arterial flow-mediated dilation after exertion involves hydrogen peroxide in overweight and obese adults following aerobic exercise training, J. Hypertens. 34 (7) (2016) 1309–1316.
[31] R. Sarfstein, Y. Gorzalczany, A. Mizrahi, et al., Dual role of Rac in the assembly of NADPH oxidase, tethering to the membrane and activation of p67phox: a study based on mutagenesis of p67phox-Rac1 chimeras, J. Biol. Chem. 279 (16) (2004) 16007–16016.
[32] Y.M. Yang, A. Huang, G. Kaley, et al., eNOS uncoupling and endothelial dysfunction in aged vessels, Am. J. Physiol. Heart Circ. Physiol. 297 (5) (2009) H1829–H1836.
[33] G.M. Reaven, Insulin resistance: the link between obesity and cardiovascular disease, Med. Clin. N. Am. 95 (5) (2011) 875–892.
[34] L. Li, S.W. Watts, A.K. Banes, et al., NADPH oxidase-derived superoxide augments endothelin-1-induced venoconstriction in mineralocorticoid hypertension, Hypertension 42 (3) (2003) 316–321.
[35] R.A. Beswick, A.M. Dorrance, R. Leite, et al., NADH/NADPH oxidase and enhanced superoxide production in the mineralocorticoid hypertensive rat, Hypertension 38 (5) (2001) 1107–1111.
[36] G.R. Drummond, C.G. Sobey, Endothelial NADPH oxidases: which NOX to target in vascular disease? Trends Endocrinol. Metab. 25 (9) (2014) 452–463.
[37] K.D. Martyn, L.M. Frederick, K. von Loehneysen, et al., Functional analysis of Nox4 reveals unique characteristics compared to other NADPH oxidases, Cell Signal. 18 (1) (2006) 69–82.
[38] R. Breton-Romero, C. Gonzalez de Orduna, N. Romero, et al., Critical role of hydrogen peroxide signaling in the sequential activation of p38 MAPK and eNOS in laminar shear stress, Free Radic. Biol. Med. 52 (6) (2012) 1093–1100.
[39] J.D. Van Buul, M. Fernandez-Borja, E.C. Anthony, et al., Expression and localization of NOX2 and NOX4 in primary human endothelial cells, Antioxid. Redox Signal. 7 (3–4) (2005) 308–317.
[40] C.P. Judkins, H. Diep, B.R. Broughton, et al., Direct evidence of a role for Nox2 in superoxide production, reduced nitric oxide bioavailability, and early atherosclerotic plaque formation in ApoE-/- mice, Am. J. Physiol. Heart Circ. Physiol. 298 (1) (2010) H24–H32.
[41] M.C. Wendt, A. Daiber, A.L. Kleschyov, et al., Differential effects of diabetes on the expression of the gp91phox homologues nox1 and nox4, Free Radic. Biol. Med. 39 (3) (2005) 381–391.
[42] T.J. Guzik, J. Sadowski, B. Guzik, et al., Coronary artery superoxide production and

nox isoform expression in human coronary artery disease, Arterioscler. Thromb. Vasc. Biol. 26 (2) (2006) 333–339.
[43] A.N. Lyle, N.N. Deshpande, Y. Taniyama, et al., Poldip2, a novel regulator of Nox4 and cytoskeletal integrity in vascular smooth muscle cells, Circ. Res. 105 (3) (2009) 249–259.
[44] R.L. Sutliff, L.L. Hilenski, A.M. Amanso, et al., Polymerase delta interacting protein 2 sustains vascular structure and function, Arterioscler. Thromb. Vasc. Biol. 33 (9) (2013) 2154–2161.
[45] L. Serrander, L. Cartier, K. Bedard, et al., NOX4 activity is determined by mRNA levels and reveals a unique pattern of ROS generation, Biochem. J. 406 (1) (2007) 105–114.
[46] R. Breton-Romero, S. Lamas, Hydrogen peroxide signaling in vascular endothelial cells, Redox Biol. 2 (2014) 529–534.
[47] D.C. Salo, S.W. Lin, R.E. Pacifici, et al., Superoxide dismutase is preferentially degraded by a proteolytic system from red blood cells following oxidative modification by hydrogen peroxide, Free Radic. Biol. Med. 5 (5–6) (1988) 335–339.
[48] D.C. Salo, R.E. Pacifici, S.W. Lin, et al., Superoxide dismutase undergoes proteolysis and fragmentation following oxidative modification and inactivation, J. Biol. Chem. 265 (20) (1990) 11919–11927.
[49] L.M. Casano, L.D. Gomez, H.R. Lascano, et al., Inactivation and degradation of CuZn-SOD by active oxygen species in wheat chloroplasts exposed to photo-oxidative stress, Plant Cell Physiol. 38 (4) (1997) 433–440.
[50] J.S. Beckman, W.H. Koppenol, Nitric oxide, superoxide, and peroxynitrite: the good, the bad, and ugly, Am. J. Physiol. 271 (5 Pt 1) (1996) C1424–C1437.
[51] H. Ischiropoulos, Biological tyrosine nitration: a pathophysiological function of nitric oxide and reactive oxygen species, Arch. Biochem. Biophys. 356 (1) (1998) 1–11.
[52] I. Mohiuddin, H. Chai, P.H. Lin, et al., Nitrotyrosine and chlorotyrosine: clinical significance and biological functions in the vascular system, J. Surg. Res. 133 (2) (2006) 143–149.
[53] G. Peluffo, R. Radi, Biochemistry of protein tyrosine nitration in cardiovascular pathology, Cardiovasc. Res. 75 (2) (2007) 291–302.
[54] L. Thomson, 3-nitrotyrosine modified proteins in atherosclerosis, Dis. Markers (2015) 708282.